Internal geometry of fault damage zones in interbedded siliciclastic sediments

TORD ERLEND SKEIE JOHANSEN[1] & HAAKON FOSSEN[2]

[1]*StatoilHydro, Post Office Box 7200, 5020 Bergen, Norway (e-mail: tesj@statoilhydro.com)*

[2]*Centre of Integrated Petroleum Research, University of Bergen, Allégaten 41, N-5007 Bergen, Norway*

Abstract: The geometry, orientation and distribution of deformation bands and fractures in eolian sandstones, siltstones and shales of the San Rafael Desert and Moab Fault area have been investigated. The results show that deformation bands, which are cataclastic in eolian sandstones and disaggregation structures in siltstones, are unevenly distributed throughout the damage zone in the form of individual bands, deformation band zones and deformation band clusters. The density of bands increases with increasing grain size. In thin (<3 m) eolian sandstones deformation band frequency is significantly lower than in thicker eolian sandstones, whereas above this thickness the frequency seems not to be related to layer thickness. Furthermore, large faults do not develop higher concentrations of deformation bands. Somewhat simplified, this suggests that damage zone growth occurs by expansion into its hanging wall and footwall. Still, the highest concentrations of deformation bands occur close to the main fault, which is of importance when considering their effect on fluid flow. Their general fault-parallel conjugate arrangements favour intra-damage zone flow parallel to rather than perpendicular to the fault.

Faults and fault-related structures and processes in porous sandstone have received growing attention during the last couple of decades (e.g., Underhill & Woodcock 1987; Fowles & Burley 1994; Antonellini & Aydin 1995; Davis 1999; Beach *et al.* 1999; Wibberley *et al.* 2000; see Fossen *et al.* 2007 for a review). It has been shown that the process of faulting is different in siliciclastic rocks compared with non-porous crystalline rocks. In particular, sandstones tend to undergo a phase of deformation band nucleation and growth prior to faulting. The hydromechanical properties of the deformation bands in many cases are such as to prohibit or restrict fluid flow. Hence, understanding the orientation, sizes, geometry, spatial distribution and properties of deformation bands around faults is of major interest, in particular to the petroleum industry (e.g., Hesthammer & Fossen 2000).

Faults in siliciclastic sediments consist of two main architectural elements that include a central fault core and an enveloping fault damage zone (Caine *et al.* 1996). The fault core absorbs most of the deformation and may contain cataclastic rocks, deformation bands, slip surfaces, lens-shaped bodies of host-rock and clay/shale smears (e.g., Shipton & Cowie 2001, 2003). The fault damage zone includes the population of brittle, fault-related deformation structures outside the fault core and may include different types of deformation bands, shear fractures and joints. Strain within the damage zone is considerably lower than in the fault core.

Deformation bands are millimetre-wide structures that characterize small-scale strain localization in porous granular media, notably in porous sandstones. Deformation bands differ from faults or slip surfaces in that they lack a discrete fracture surface. Furthermore, most deformation bands maintain or increase cohesion, while cohesion is lost across classical fractures. Formation of deformation bands normally involves compaction and reduction of porosity, whereas dilation may occur along restricted sections of the bands, such as in the tip region (Antonellini *et al.* 1994). Only in rare cases do dilational bands occur (Du Bernard *et al.* 2002). Deformation bands are classified based on kinematics (Aydin *et al.* 2006) or deformation mechanisms (Fossen *et al.* 2007). Disaggregation bands form by grain boundary sliding and granular flow and accommodate minor reduction in porosity (Fisher & Knipe 1998; Hesthammer & Fossen 2001). Formation of cataclastic deformation bands involves grain comminution, which in turn results in reduction of grain size and porosity relative to the host rock (Antonellini *et al.* 1994; Marone and Scholz 1989; Menéndez *et al.* 1996; Hadizadeh & Johnson 2003). In mica-, chlorite- and clay-bearing sandstones, phyllosilicate grains reorient and align with the deformation bands, forming a framework structure in the sandstone across which fluid flow is restricted. These

From: WIBBERLEY, C. A. J., KURZ, W., IMBER, J., HOLDSWORTH, R. E. & COLLETTINI, C. (eds) *The Internal Structure of Fault Zones: Implications for Mechanical and Fluid-Flow Properties*. **299**, 35–56.
DOI: 10.1144/SP299.3 0305-8719/08/$15.00

structures are known as framework phyllosilicate bands (Knipe *et al.* 1997; Fisher & Knipe 1998). In addition, temperature history is an important control on the dissolution and cementation of quartz and other minerals and may influence the sealing potential of faults and deformation bands (Hesthammer *et al.* 2002; Fisher *et al.* 2003).

Granular flow dominates at shallow burial depths (<1 km) and low confining pressure in poorly consolidated sands (Owen 1987; Fisher & Knipe 1998). Grain comminution and quartz dissolution/cementation dominate in consolidated sands at deeper burial depths (>1 km) and higher confining pressures, although studies have shown that cataclasis may also occur under low confining pressure in unconsolidated sediments (Cashman & Cashman 2000; Rawling & Godwin 2003). Lithological factors, such as sorting, roundness, grain size and composition, are also important in controlling the deformation mechanisms under given boundary conditions.

Aydin (1978) and Aydin & Johnson (1978) presented the now widely accepted model that faults in porous sandstones typically grow from swarms of deformation bands, which result from strain hardening during the growth history of single deformation bands (Schultz & Siddharthan 2005, cf. Harper & Lundin 1997). This model explains why deformation bands never accumulate more than centimetre-scale displacements before interlocking of grains and related strain hardening cause strain to relocalize by the formation of a new band(s) in their vicinity. The faulted deformation band model has been supported by other field studies (Antonellini & Aydin 1995; Fossen & Hesthammer 1997; Shipton & Cowie 2003) as well as experimental work (Mair *et al.* 2000).

In this paper we revisit the field area in the San Rafael Desert of SE Utah (Fig. 1a), where faulting in porous sandstones was first explored in detail (Aydin 1978; Aydin & Johnson 1978, 1983), and we examine a system of small normal faults and fault-related structures (<15 m throw) that offset interbedded sandstones, siltstones and shales of the Entrada and Carmel Formations. In addition, field data from a major (about 200 m throw) fault segment related to the Moab Fault (Fig. 1b) (Foxford *et al.* 1996) in the Paradox Basin are presented. The objective of the current study is to identify internal geometrical characteristics of fault damage zones in multi-layered siliciclastic rocks. Seven fault zones that offset interbedded eolian sandstones, siltstones and shales have been examined and mapped in detail using surface grids and fault-perpendicular scanlines.

Geological setting

The San Rafael Desert area

The San Rafael Desert study area (Fig. 1a) is situated off the SE flank of the San Rafael Swell, one of several Late Cretaceous–early Tertiary Laramide-related contractional uplift structures on the Colorado Plateau (e.g., Bump & Davis 2003). The Jurassic stratigraphic framework of the San Rafael Desert study area (Fig. 1c) is dominated by interlayered fluvial, tidal and sand dune deposits (Milligan 2000) assigned to the Upper Member of the Carmel Formation and the Middle Jurassic Entrada Formation. The Upper Member of the Carmel Formation contains alternating red siltstone to silty, very fine sandstone, shales, and light-coloured, medium grained quartz arenites resting on top of thick alabaster gypsum interbedded with shale. The Entrada Formation is 76–160 m thick and sub-horizontal across most of the San Rafael Desert study area. Four sub-units have been discerned in ascending stratigraphic order: e_1, e_2, e_3 and e_4. Sub-units e_1 and e_3 and e_4 are dominated by light-coloured massive or cross-laminated, medium-grained quartz arenites (dune deposits), whereas sub-unit e_2 constitutes red-brown siltstone to very fine-grained sandstone in alteration with thin shales. The siltstones, shales and sandstones of the Carmel Formation are texturally similar to those of the Entrada Formation. Layer-internal variation in grain-size from that of the siltstones to the very fine-grained sandstones is common. For convenience, however, these lithologies are referred to as siltstones in the remainder of this paper.

The faults examined belong to a regional system of NW–SE-oriented normal faults (Aydin & Johnson 1978, 1983) that accommodate minor NE–SW extension and cut across the San Rafael Swell (Milligan 2000). The general fault pattern locally defines orthorhombic fault blocks in plan view (Aydin & Reches 1982).

The cross-cutting relationship between the extensional faults and the San Rafael Swell indicates that the extension postdates the Laramide contraction. During this period the Jurassic units in the Paradox Basin, about 90 km to the east, were buried at about 2 km depth (Nuccio & Condon 1996; Garden *et al.* 2001).

The Moab area and the Moab fault

In the Moab area, about 90 km east of the San Rafael Desert study area, the Entrada Formation is represented by the approximately 60 m thick Slickrock Member (Fig. 1b). The Slickrock Member is a fine-grained, cross-laminated eolian sandstone with local silty to very fine-grained interdunes. The

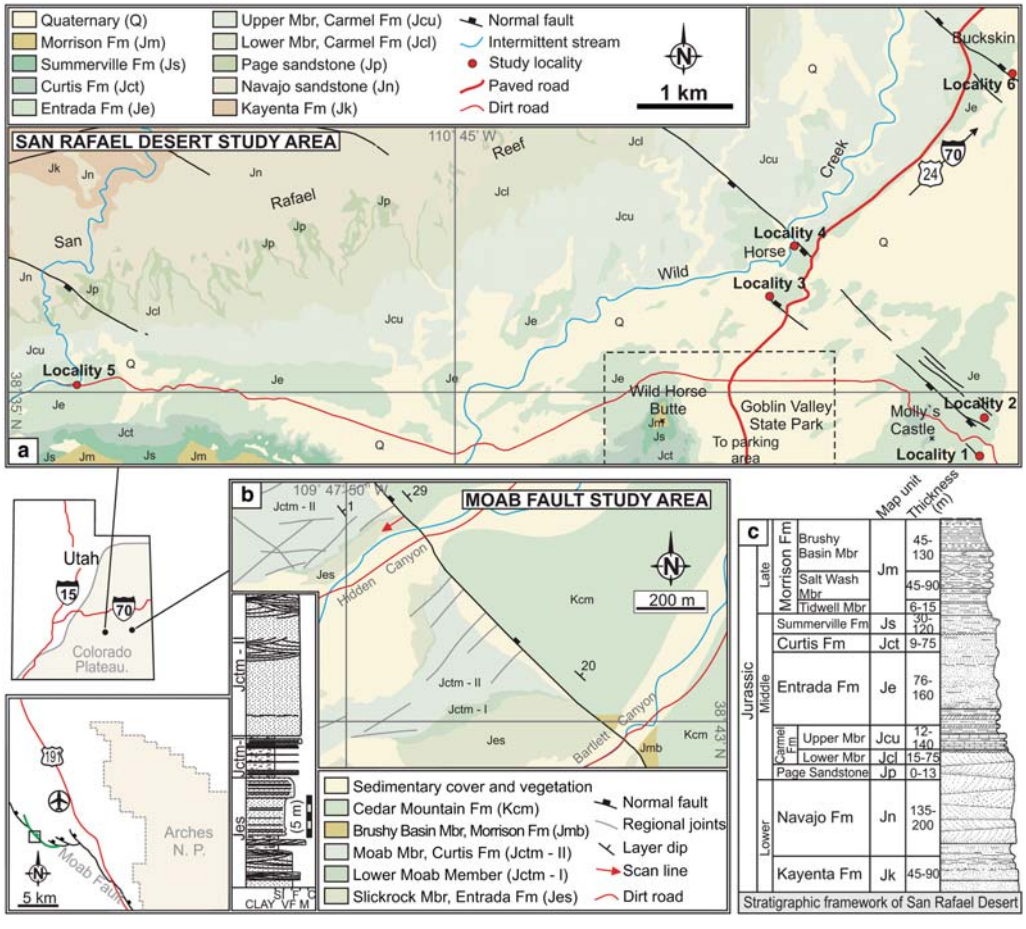

Fig. 1. Overview of study areas. (**a**) San Rafael Desert. (**b**) The Bartlett Fault (solid green line) comprises one of several fault segments connected to the northwestern end of the Moab Fault. Only the most significant regional joints are shown. (**c**) Stratigraphic column of the San Rafael Desert. Modified from Doelling (2001, 2002).

Slickrock Member is overlain by the Moab Member of the Curtis Formation (Doelling 2000). The Moab Member is 25–30 m thick and consists of a light-coloured, massive, medium-grained eolian sandstone unit, underlain by a few-metres-thick siltstone. These and other units are locally affected by the Moab Fault (Fig. 1b), which is structurally located within the Paradox Fold and Fault Belt (Doelling 1988). The Moab Fault defines a major NW-striking, salt-related normal fault with a total outcrop length of about 45 km and a maximum throw of about 950 m (Foxford *et al.* 1996). The northern part of the Moab Fault splays into a series of west-stepping, hard-linked fault strands which will be discussed below.

Salt diapirism in the Moab area was triggered by reactivation of basement lineaments in the Permian–Triassic, which also caused the creation of the Moab Fault in sediments overlying the Paradox salt (Foxford *et al.* 1996). The age of the Moab Fault itself is uncertain, but K–Ar (Pevear *et al.* 1997) and Ar/Ar dating (Solum *et al.* 2005) indicate that much of its present offset accumulated during the late Cretaceous–early Tertiary (Laramide) time period. This was also the time of maximum burial, implying that faulting of the Entrada Sandstone occurred at burial depths of approximately 2.2 km (Nuccio & Condon 1996; Garden *et al.* 2001).

Outline of structural data

Deformation structures

Faults in the eolian sandstones of the study region are associated with abundant cataclastic

deformation bands (Fig. 2a & b) with offset and width in the order of 0–40 and 0.5–2 mm, respectively. At the microscale, these deformation bands show evidence of extensive grain comminution accompanied by reduced grain size and collapse of pore space (Aydin 1978; Aydin & Johnson 1978; Antonellini *et al.* 1994). The deformation bands appear as isolated bands or define densely

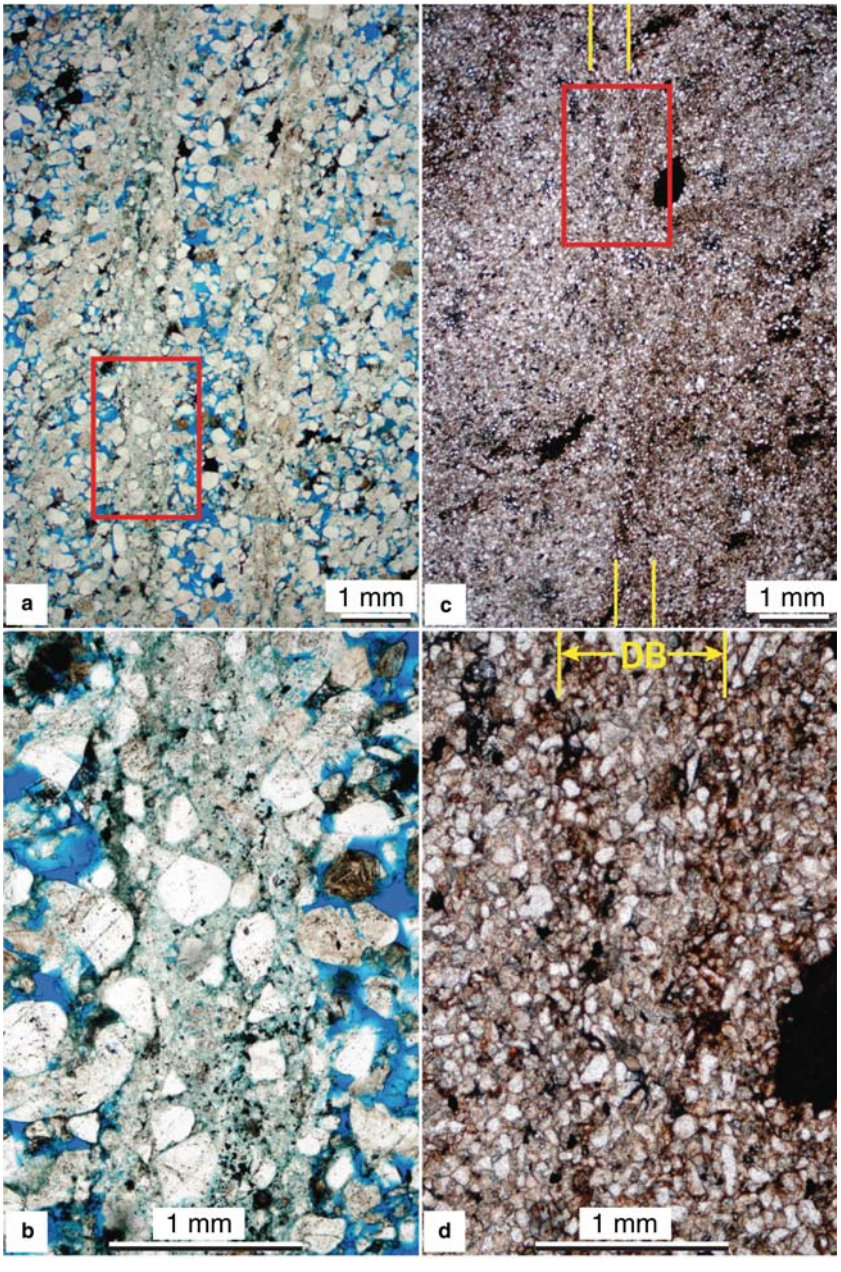

Fig. 2. Deformation bands in the study area. (**a**) Cataclastic deformation band where grain crushing (cataclasis) has resulted in grain-size reduction and a dense, low-porosity band about 1mm thick. (**b**) Magnification of the field indicated in (a). (**c**) Disaggregation band in siltstone. Deformation occurred by grain reorganization (granular flow), and no grain-size reduction is seen and the deformation occurred by grain reorganization (granular flow). (**d**) Magnification of the field indicated in (c).

packed tabular zones of bands. Bands within the decimetre-thick zones show anastomosing arrangement along strike. Deformation bands and deformation band zones may also be concentrated at larger scales as clusters 1–10 m wide. Such concentrations are here referred to as deformation band clusters and represent concentrations within fault damage zones.

Deformation bands in the siltstones of the study region have widths of less than 0.5 mm (Fig. 2c & d) and offsets of up to several tens of centimetres. Their microstructure reveals generally fine-grained, well-sorted and quartz-rich gouge with minor phyllosilicate content. Grain comminution and reduction in grain size is weak or absent, i.e., cataclasis appears much less prominent as compared with deformation bands in the eolian sandstones (Fig. 2a & b). Deformation bands in the siltstones thus classify as disaggregation bands.

In the shales the deformation bands are replaced by shale smears or slip surfaces, which can be hard to detect in outcrop. Those observed occur close to major slip surfaces or along the vertical continuation of thick zones of deformation bands in the eolian sandstones. None of these non-cohesive structures were sampled.

Slip surfaces occur in all three lithologies. In the eolian sandstones they are associated with tabular zones of densely packed deformation bands (Aydin 1978; Aydin & Johnson 1978; Antonellini *et al.* 1994), while in the siltstones they may occur as more or less isolated structures or accompanied by a few disaggregation bands. Slip surface represents the main structure type in the shales.

San Rafael Desert study localities

The San Rafael Desert study area is situated close to the Goblin Valley State Park and features an array of small-scale, NW–SE-oriented steeply (65–80°) dipping normal faults with throw up to 15 m (Fig. 1a). Fault damage zones were mapped at six localities in the Entrada and Carmel Formations (Figs 3–6).

Locality 1 (Fig. 3a) shows a vertical section across a minor normal fault which offsets two thick eolian sandstone beds separated by a 0.5 m thick shale, all assigned to the Entrada Formation, by 1.7 m. The fault core displays a throughgoing slip surface mantled by 10–20 cm thick deformation band zones. The slip surface is oriented at 144/69 (right-hand rule used throughout this paper) and shows dip–slip striations with a minor sinistral component (pitch: 77°E). Scan-line data were recorded across the fault in the shale and the lower eolian sandstone bed. The results are rendered in Figures 7a, b & 8a.

Locality 2 (Fig. 3b) features two sub-parallel normal faults (Faults 1 and 2) that penetrate sandstones, siltstones and shales of the Entrada Formation, all surrounded by deformation bands of synthetic and antithetic dips. Fault 1 defines a geometrically coherent and sub-planar slip surface oriented at 121/80, whereas Fault 2 consists of several hard-linked slip surface segments with strike in the range of 099–128° and about 80° dip. Segment interaction has resulted in metres-wide deformation band networks in unit e_3 (Fig. 3b), each containing hundreds of deformation bands and several minor slip surfaces. Structural data were sampled along a fault-perpendicular exposure to the NW and include two scanlines in eolian sandstone (units e_1 and e_3), two scanlines in siltstone (e_2) and two scanlines in shale (e_2). The results are shown in Figures 7c–h & 8b–f. Here, the offsets of Faults 1 and 2 approximate the maximum offsets, estimated to 3.1 and 5.4 m, respectively. Throw decreases toward the SE, where all structures disintegrate into an array of deformation bands (unit e_3).

The normal fault in Locality 3 (Fig. 4a) was examined by Schultz & Fossen (2002) and offsets siltstones and shales of the uppermost Carmel Formation (Upper Member) as well as a thick, light-coloured and medium grained eolian sandstone of the lowermost Entrada Formation (e_1). The fault core is associated with a throughgoing, striated slip surface and centimetres-thick gouge, which is mantled by a sub-parallel deformation band zone in the Entrada Formation The main slip surface is oriented at 313/69 and has about 6 m offset in the examined cross-section. Structural data were acquired from fault-perpendicular scanlines in the three lithologies. The results are shown in Figures 7i–k & 8g–h.

Locality 4 (Fig. 4b) exposes a steep, SE-striking (133/78) normal fault with a fault core comprising centimetres-thick, dark-coloured gouge and a throughgoing striated slip surface with about 15 m offset. The outcrop lithology is similar to that of Locality 3 and features a light yellow, medium-grained eolian sandstone of the Entrada Formation (e_1) resting on top of alternating sandstones, siltstones and shales of the Carmel Formation. More heterolithic sequences of evaporates, siltstones and shales (Doelling 2002) characterize the stratigraphically deepest exposures of the Carmel Formation. Here, the fault passes into a monoclinal flexure associated with steep minor reverse and normal faults. Structural scanline data were recorded from two separate sandstones and a siltstone, about 5 m into the hanging wall. The results are provided in Figures 7l–n & 8i–k.

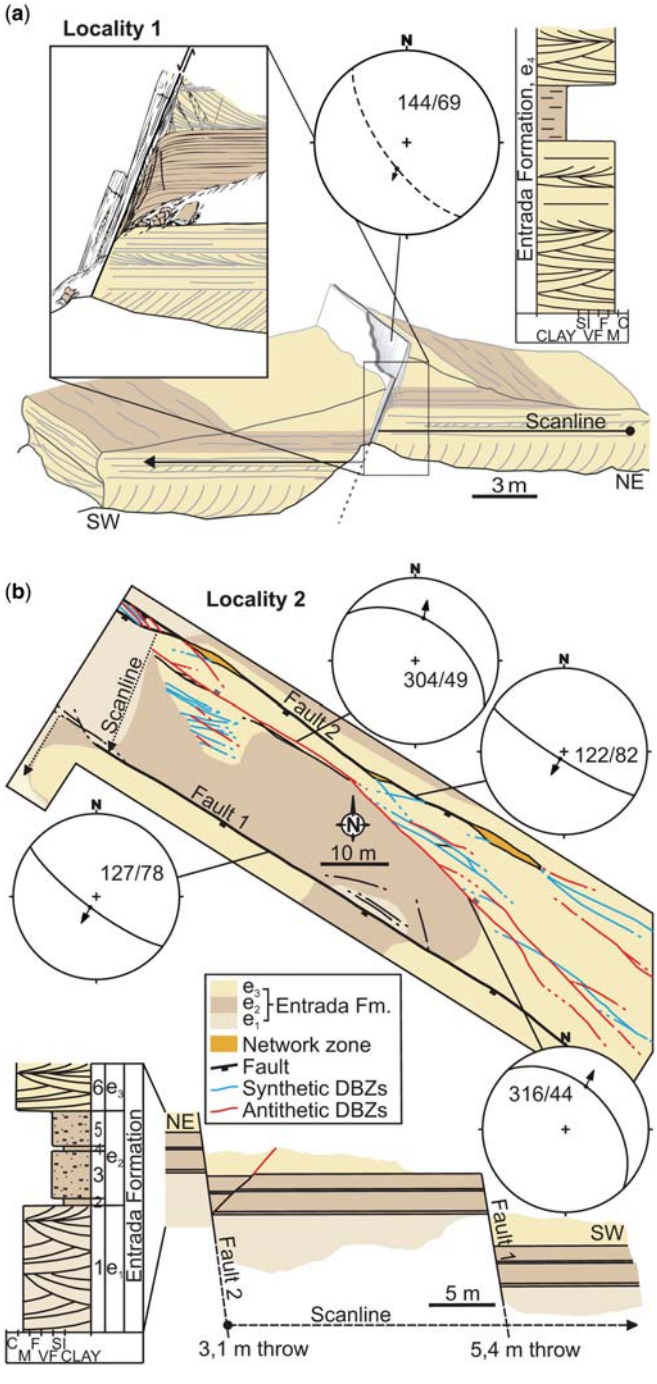

Fig. 3. Outcrops of faults in the Entrada Formation close to the Molly's Castle in the southeastern part of the San Rafael Desert study area. (**a**) Locality 1 features an isolated normal fault offsetting eolian sandstone and shale by about 1.7 m. Deformation bands and fractures were recorded along indicated scanline. (**b**) Locality 2 shows two sub-parallel normal faults that cut across sandstones, siltstones and shales. Fault orientations and pitch of striations are projected in equal area stereoplots (lower hemisphere). Structural data were recorded in all lithologies along scanlines and from surface grids (unit e_3). Synthetic (blue) and antithetic (red) deformation band zones (DBZs) are outlined in the upper sandstone (e_3), and the colour code corresponds to that of Figure 8c. The largest deformation band zones continue as slip surfaces in the siltstones and shales.

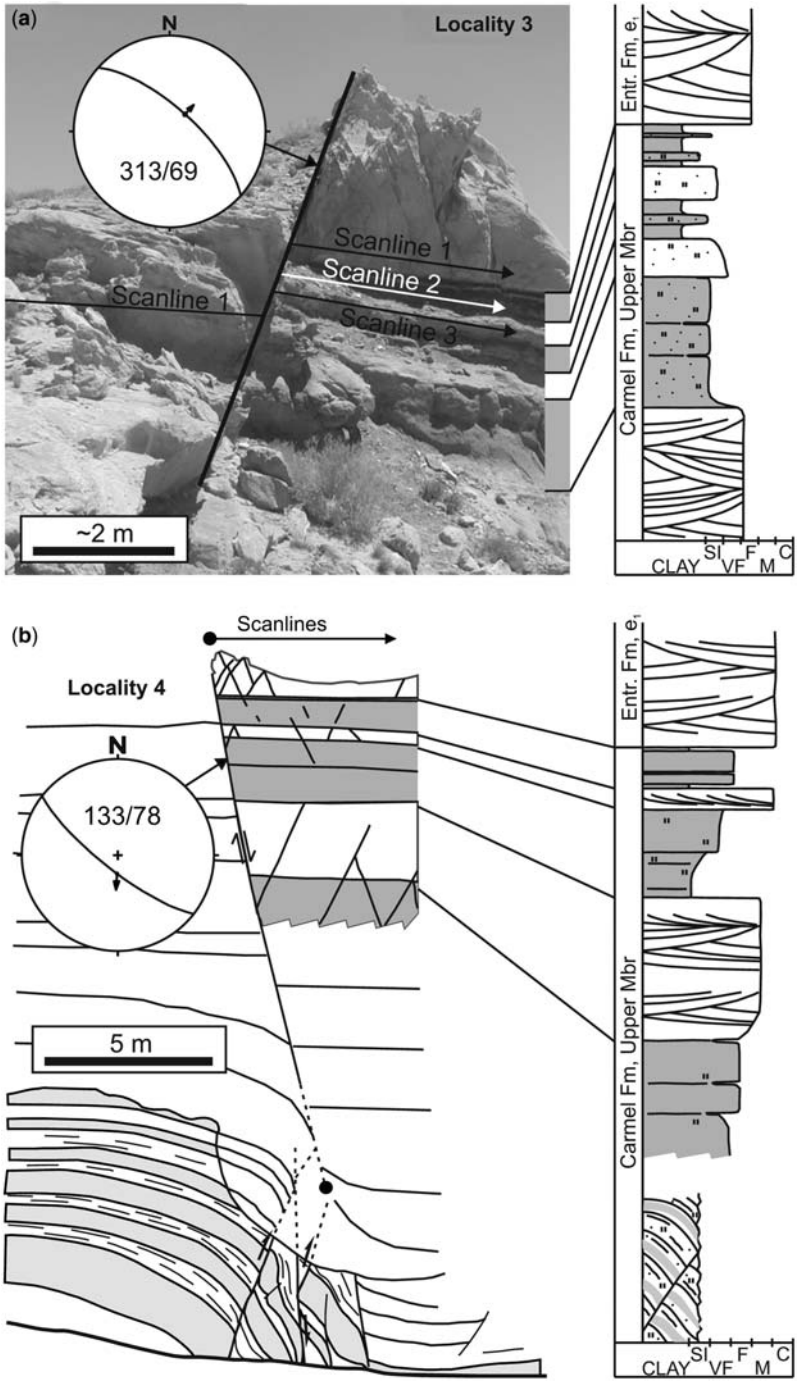

Fig. 4. Localities near the Wild Horse Creek in the San Rafael Desert study area showing faults in the Entrada and Carmel Formations. (**a**) Normal fault in Locality 3 with offset of about 6 m. Structural data were recorded along three scanlines in eolian sandstone, siltstone and shale. (**b**) Normal fault in Locality 4 with about 15 m offset. Fault-related structures were mapped in similar lithologies as in Locality 3 along scanlines extending about 5 m into the hanging wall. Fault orientations and pitch of striations are projected in equal area stereoplots (lower hemisphere).

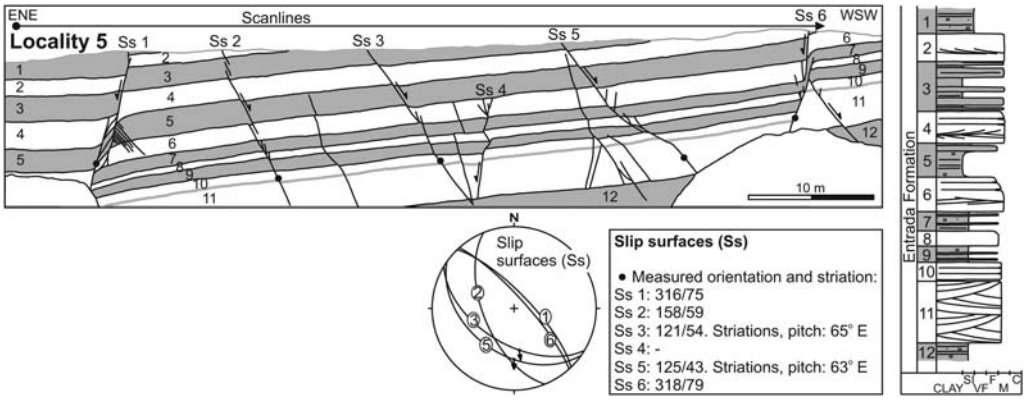

Fig. 5. Locality 5 at the Little Wild Horse Canyon trailhead in the San Rafael Desert. Several small faults (slip surfaces = Ss) with offset in the range 0.1–1.9 m crop out in 70 m wide and 10 m high ENE–WSW oriented vertical cross-section. The orientation of the faults and associated slickenline striations are shown in the stereoplot, whereas the respective sample locations are indicated in the cross-section (black dots). Deformation bands and slip surfaces were mapped in eight separate lithological units, constituting interbedded sandstone, siltstone and shale of the Entrada Formation.

Locality 5 (Fig. 5) features an array of small faults that crop out in the Entrada Formation along a 70 m wide and 10 m high ENE–WSW oriented vertical cross-section. These faults exhibit a NW–SE orientation and have offset in the range of 0.1–1.9 m. Data were sampled along scanlines in eight separate lithological units, constituting layers of sandstone, siltstone and shale (Fig. 9).

Locality 6 (Fig. 6) exposes two overlapping NE-striking faults, which penetrate the Entrada and Carmel Formations. The largest fault (Fault 1) is mainly dip–slip with an orientation of about 300/70 and maximum offset of approximately 12 m. Fault 2 is near vertical and oriented at 292/80. Slip surface striations demonstrate prominent dextral slip with pitch in the range of 10–49°E (31°E average). The overlap zone covers a 100 by 250 m area, breached by abundant oblique faults. Slickenside striations were measured on slip surfaces within the overlap zone, and deformation bands along one of the breaching faults were mapped in detail. In addition, scanline data were sampled in unit e_3 perpendicular to Fault 1, SE of the overlap zone (Figs 7o & 8l).

The Moab Fault

Structural analyses of the Moab Fault area were carried out along one of the major NW-striking fault segments connected to its northwestern end (Fig. 1b), known as the Bartlett Fault (Fossen *et al.* 2005). Fault-perpendicular canyons, such as the Hidden Canyon, expose outstanding sections through the fault segment. The fault displacement is close to 200 m in the Hidden Canyon area, and the fault core is locally up to 5 m wide and defines a composite extensional duplex of cataclastic fault rocks, major fault-bounded lenses of host rock and numerous slip surfaces. Strata in the hanging wall are affected by a 200–300 m wide syncline with a maximum layer dip of 20–30° adjacent to the fault core. The layering in the footwall is sub-horizontal.

Deformation band distribution and orientations were sampled in the footwall from the Moab Member and Slickrock Member in Hidden Canyon (Figs 10 & 11). In the Slickrock Member two sub-layers were examined, including a medium-to coarse-grained eolian sandstone layer and a fine-grained to silty interdune layer, both with thicknesses of 0.5–1.0 m. Deformation bands in these lithologies are similar to those of corresponding lithologies in the San Rafael Desert study area (Aydin 1978). Light-coloured, 1–2 mm wide cataclastic bands reside in the eolian sandstone units, whereas narrow (<0.5 mm), dark-coloured disaggregation bands are seen in the interdune deposits. The dark brownish colour of the disaggregation bands is related to iron (hydr)oxides rather than to phyllosilicates (which are absent or scarce in the interdune siltstones). In addition to deformation bands, all lithologies contain a small number of slip surfaces. Sub-vertical, regional joints cut across and postdate the damage zone, but do not significantly bias deformation band frequencies associated with the Bartlett Fault due to their wide spacing (5–30 m).

Although not fully covered by the scanline, the total width of the damage zone in the Moab

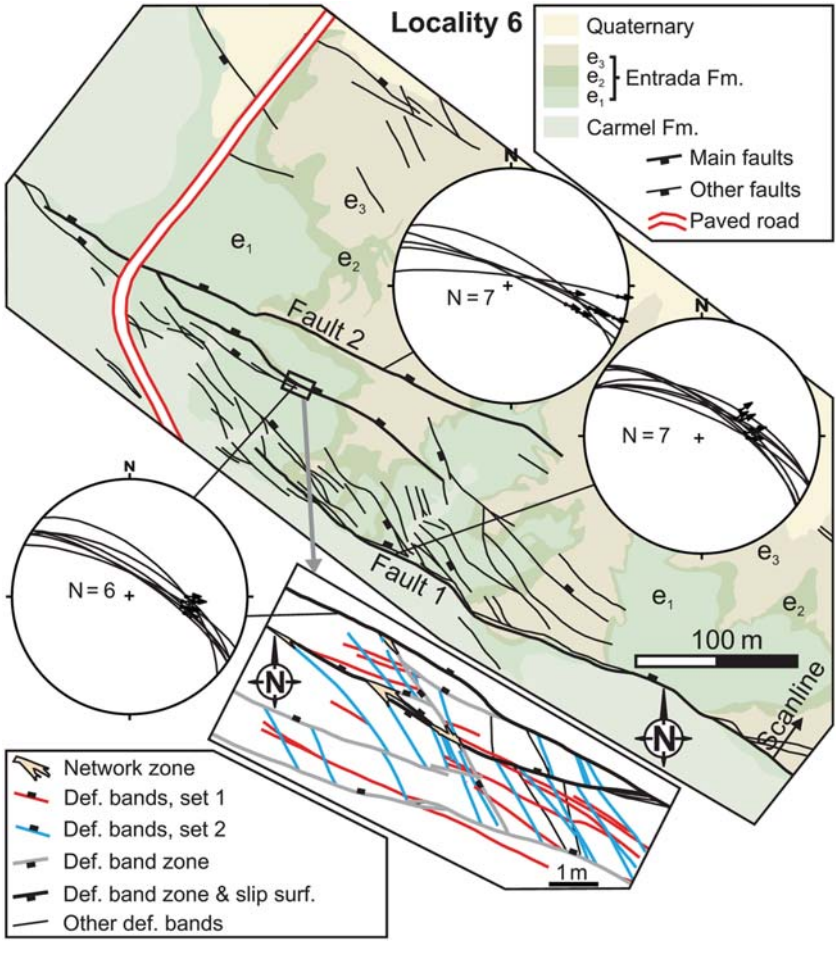

Fig. 6. Locality 6 in the San Rafael Desert show two overlapping faults (Faults 1 and 2) in the Entrada and Carmel Formations. The largest fault (Fault 1) is mainly dip–slip and has offset of approximately 12 m. Slip surface striations on Fault 2 demonstrate prominent dextral slip with pitch in the range of 10–49°E. Fault orientations are shown in stereoplots (equal area, lower hemisphere). Slip surface striations were also measured on slip surfaces within the overlap zone. Further, deformation bands along one of the breaching faults were mapped in detail (field indicated in map), and the colour code of Set 1 (red) and Set 2 (blue) corresponds to that in Figure 18c. Scanline data were sampled perpendicular to Fault 1 in unit e_3.

Member in Hidden Canyon approximates 70 m. Here, the deformation band frequency is at its maximum of about 100 m^{-1} close to the fault core, and decreases toward the margin of the damage zone (Fig. 10a). High-frequency deformation band clusters (>20–30 m^{-1}) typically envelop a throughgoing slip surface. The damage zone is much narrower in the interdune units (about 13 m wide; Fig. 10b). Deformation band frequencies are high (>70 m^{-1}) adjacent to the fault core, but decline rapidly to less than 18 m^{-1} toward the peripheral part of the damage zone. The width of the damage zone in the Slickrock Member dune is similar to that of the interdune, but the deformation band frequencies are higher (about 5 m^{-1}) on the whole (Fig. 10c). Despite significant scatter in the orientation data, the vast majority of the structures follow the trend of the main fault (318/62) (Fig. 11). Synthetic structures with sample mean orientation (316/62) close to the main fault orientation prevail in the Moab Member (Fig. 11a), while the less frequent yet abundant antithetic structures (143/75) have about 10° steeper dip on average (Fig. 11b).

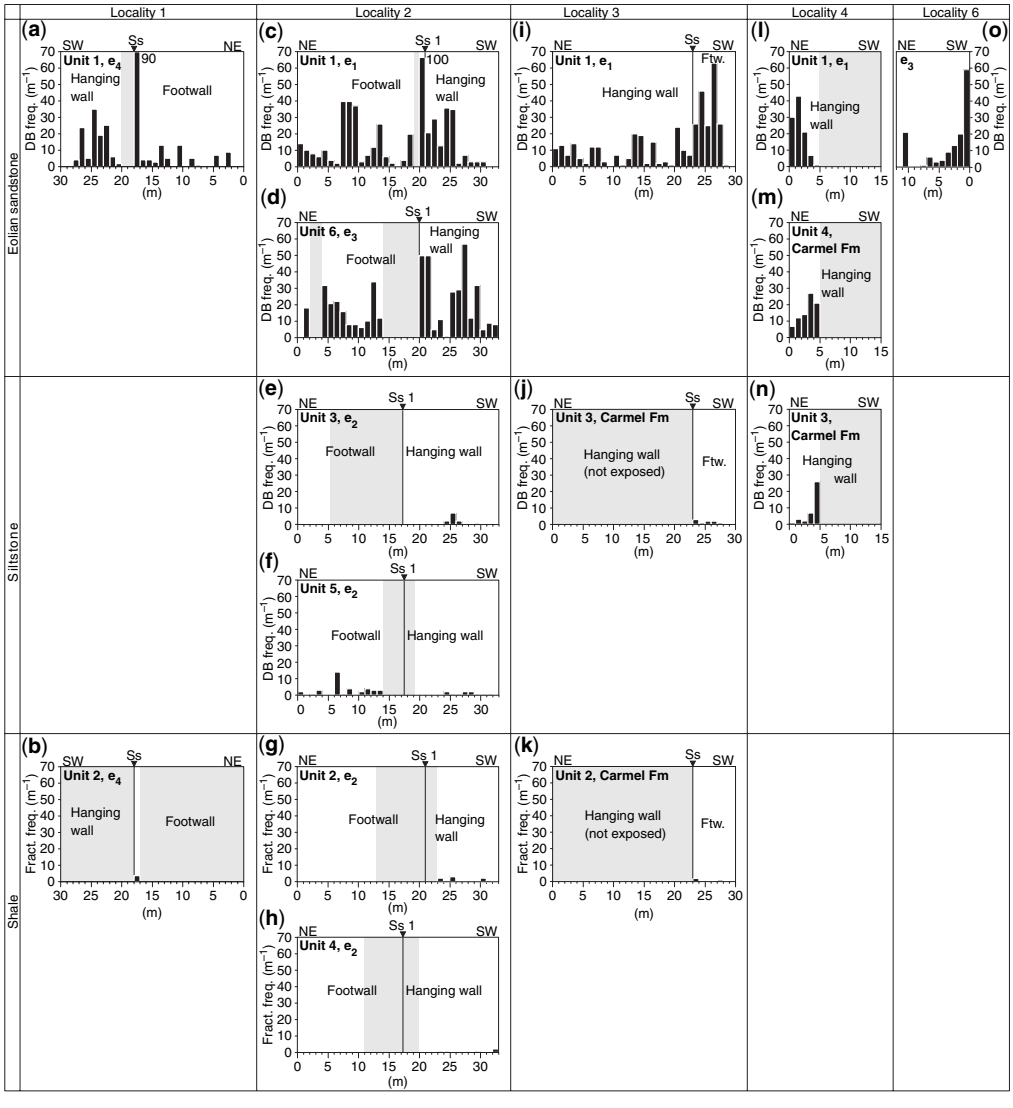

Fig. 7. The spatial distribution of deformation bands and fractures in the damage zone of faults in the San Rafael Desert area was recorded along fault-perpendicular scanlines in eolian sandstones, siltstones and shales. The resulting deformation band (DB) and fracture frequency profiles have been arranged according to lithology and locality. Grey areas indicate unexposed sections. Throughgoing slip surfaces (Ss) are indicated in the profiles. Ss 1 in Locality 2 corresponds to Fault 1 in Figure 3b.

Sub-vertical structures (dip $>80^\circ$) parallel to the main fault (Fig. 11b) are also frequent. The Slickrock Member dune and interdune units show similar deformation band orientations with two distinct sets (Fig. 11c & d). Sub-vertical deformation bands are frequent in both lithologies, but antithetic deformation bands are about 10° steeper in the interdune than in the dune units. However, synthetic deformation bands were not recorded.

Results and discussion

Deformation band frequency v. lithology

The spatial distribution of deformation bands has been recorded along 29 fault-perpendicular scanlines in porous eolian sandstones, siltstones, and shales, as shown in Figure 7 (San Rafael Desert), Figure 9 (San Rafael Desert, Little Wild Horse Canyon trailhead) and Figure 10 (Bartlett

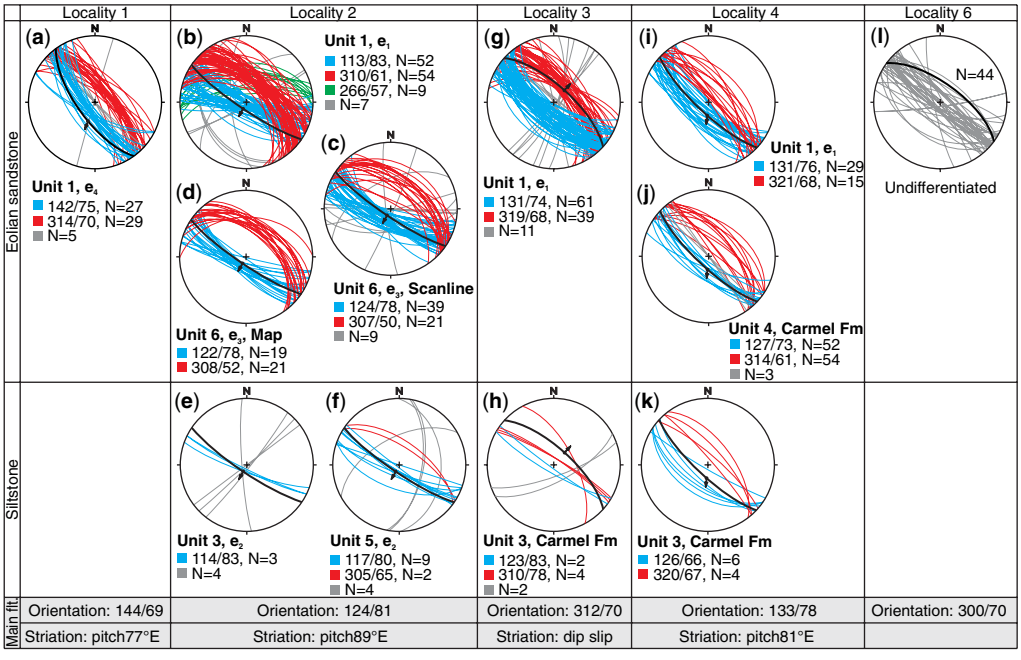

Fig. 8. Stereoplots (equal area, lower hemisphere) of deformation bands in eolian sandstones and siltstones in fault damage zones of the San Rafael Desert area. The thick black line (great circle) represents associated main fault (slip surface) orientation. Main fault orientation and pitch of striations are noted at the base of the figure. The stereoplots have been arranged with respect to location and lithology. The colour code represents the dominant sets, and their respective average orientation is as indicated.

Fault). Among several characteristic features revealed by this data set is the clustered distribution of deformation bands in the fault damage zones. The most prominent clusters appear in the eolian sandstones, manifest as up to 10 m wide zones with several tens or hundreds of deformation bands and typically also deformation band zones with opposing dips (Fig. 12). Most of these deformation band clusters, however, range in width from 2 to 7 m (Fig. 13a). Deformation band frequencies tend to reach their maxima near the centre of the clusters. Typically, the maximum deformation band frequencies are in the range $5–40\ m^{-1}$, but may locally approach $100\ m^{-1}$ (Fig. 13b). The clusters have been determined qualitatively from deformation band frequency profiles, as indicated in Figure 10a. It should be noted, however, that these data reflect concentration per measured metre, and that the concentration for instance at the 10 cm scale can be considerably higher when crossing a deformation band cluster.

An important finding is the lithological control on deformation band and fracture frequency. Clearly, the maximum deformation band frequency of clusters in the eolian sandstones is generally much higher and shows significantly greater scatter compared with that of deformation band clusters in the siltstones (Fig. 14). In the shales discrete fractures in the form of slip surfaces dominate, but fracture clusters are nearly absent. Such lithology-dependent contrasts in fault damage zones are probably attributed to contrasting fault growth mechanisms in the different lithologies. It is generally thought that sequential growth of deformation bands in response to strain hardening of gouge precedes faulting, i.e., nucleation of slip surfaces, in porous sandstones (Aydin & Johnson 1978, 1983; Jamison & Stearns 1982; Underhill & Woodcock 1987; Antonellini & Aydin 1994; Mair *et al.* 2000; Wibberley *et al.* 2000; Shipton & Cowie 2001, 2003; Rawling & Goodwin 2003; Schultz & Siddhartha 2005). Strain hardening of gouge within a deforming band results in loading of the more compliant sidewalls, in which new deformation bands may form. This model can explain the extensive deformation band zones and clusters observed in the eolian sandstones.

The thinner zones and larger offsets of disaggregation bands in siltstones suggest that strain hardening is less important or absent here. Strain hardening seems to be related to deformation

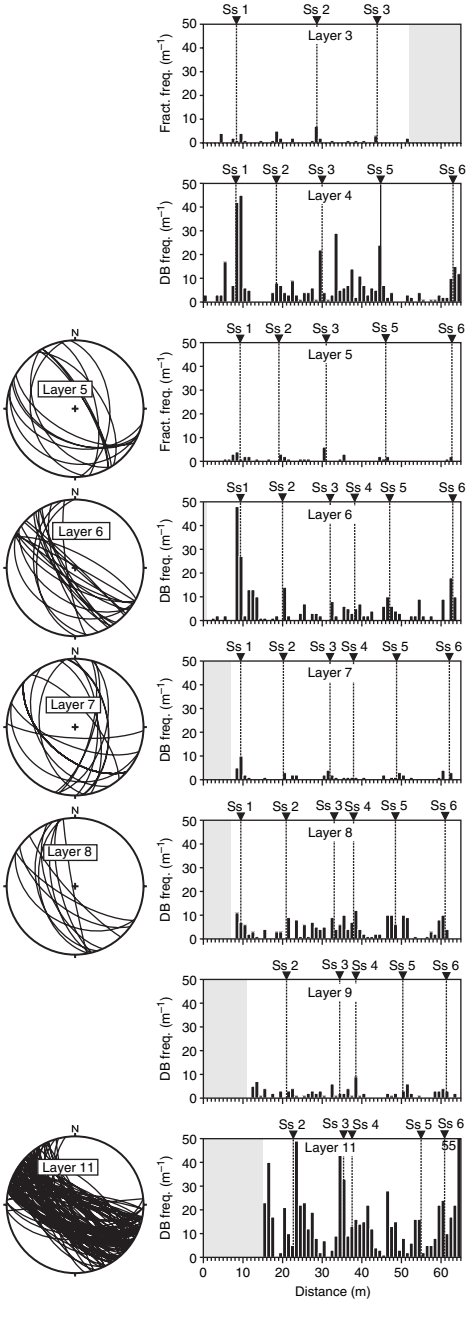

Fig. 9. Results from Locality 5. Deformation band and fracture frequencies were recorded in eight layers, including eolian sandstones, siltstones and shales. Grey areas indicate lack of exposure. Deformation bands (DB) dominate the eolian sandstones and siltstones, whereas fractures (slip surfaces) dominate the shales. Note high deformation band frequencies in the sandstones relative to that of siltstones and shales. Orientation data were recorded only in sandstones and siltstones. Stereoplots (equal area, lower hemisphere) demonstrate a relatively complex pattern, but the main trend is sub-parallel to that of the slip surfaces (Ss). The numbering of the slip surfaces as well as the layers is in accordance with Figure 5.

mechanism in this case. The disaggregation bands do not involve significant grain fracturing, probably because of the finer grain size and the resulting lower grain-contact stresses (Schultz & Siddharthan 2005; Fossen *et al.* 2007). There is no reason to believe that the reorganization of grains itself would cause significant strain hardening (Harper & Lundin 1997), although the formation of grain bridge structures may result in temporal stress fluctuations (Mandl *et al.* 1977). However, the cataclastic grain size reduction, porosity reduction and the change from rounded to angular grain shapes seen in the cataclastic deformation bands in the eolian sandstones (Fig. 2a & b) cause locking of grain contacts and thereby promote strain hardening, wider deformation band zones, and smaller offsets of deformation bands in these sandstones.

Shale layers show no evidence of sequential deformation band growth, which can probably be explained by the presence of phyllosilicates (Fisher & Knipe 1998), in addition to the fine grain size. Phyllosilicates tend to align along the shear fracture and seem to have a smearing and weakening effect as offset accumulates. Thus, strain softening and early slip surface formation occur.

Growth of deformation band clusters

The maximum deformation band frequency of the deformation band clusters in the eolian sandstones decreases non-linearly with distance to the main fault core or slip surface (Fig. 15). Hence, clusters located close to the main fault can be expected to contain considerably higher concentrations of deformation bands than more peripheral clusters. Comparing the damage zone data from the small ($<$15 m throw) faults in the San Rafael Desert area with the 200 m throw Bartlett fault reveals similar concentrations of deformation bands very close to the fault core, but higher concentrations of deformation bands in the peripheral part of the Bartlett fault damage zone relative to the San Rafael Desert faults. These characteristics indicate that new clusters form peripherally while the established clusters continue to grow. However, because clusters adjacent to the main fault have similar maximum deformation band frequencies in both wide and narrow damage zones, there seems to be

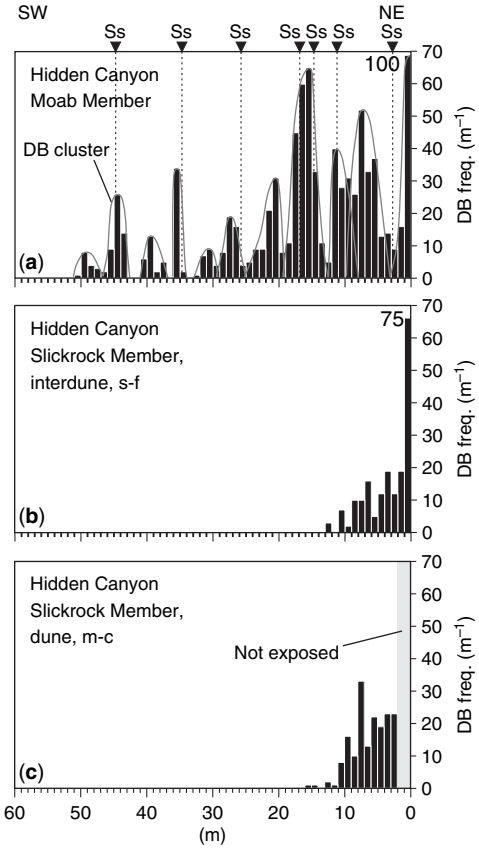

Fig. 10. Distribution of deformation bands (DB) in the footwall damage zone of the Bartlett Fault in Hidden Canyon. (**a**) Profile in Moab Member. Throughgoing slip surfaces (Ss) are indicated, and deformation band clusters are outlined. Close to the main fault the clusters tend to overlap. (**b**) Profile in Slickrock Member interdune and (**c**) dune. The deformation band and fracture frequencies in the Slickrock Member are generally lower and the fault damage zone is narrower compared with the Moab Member.

a critical strain level at which the clusters become saturated with deformation bands. Based on the plot in Figure 15, this critical strain level corresponds to a deformation band frequency of about 100 m^{-1} in the study area.

In the eolian sandstones the maximum deformation band frequency associated with slip surfaces is typically about 25–60 m^{-1}, but may be as high as 100 m^{-1}. The largest clusters are frequently associated with a throughgoing slip surface. For example, slip surfaces in the San Rafael Desert are commonly centred within the largest clusters (Fig. 7), and several of the subsidiary slip surfaces in the footwall of the Bartlett fault are mantled by major deformation band clusters (Fig. 10a). If, as suggested by Aydin & Johnson (1978), deformation band formation involves strain hardening and faulting implies strain softening in these rocks, then there is no mechanical reason why deformation bands should form after the establishment of a continuous slip surface. However, the variation in deformation band density around slip surfaces is considerable. Whether this variation is related to local lithological changes or stress perturbations, or whether deformation band growth occurs near the slip surface at a later stage, is not evident from our data. Renewed deformation band growth could be related to incorporation of fault lenses or geometrical asperities along the slip surface. However, it is unclear why higher deformation band concentrations should be obtained during faulting preferentially to forming new slip surfaces in the wall rock. Hence, it seems likely that the maximum concentration of deformation bands near slip surfaces for the most part is established prior to faulting of the deformation band zone.

Several studies have shown a positive correlation between damage zone width and main fault offset for porous sandstones (e.g., Beach *et al.* 1999; Shipton & Cowie 2001). The widths of the damage zones are generally not well constrained in the current study, owing to limited exposure or interference of damage zones of adjacent faults. Accordingly, such correlations have not been possible to study directly, although Figure 15 may suggest a positive correlation. Field observations do, however, show that the width of damage zones is prone to considerable variation along strike even within the same lithology.

There is a non-linear correlation between the total number of deformation bands within the clusters and their respective widths (Fig. 16). More precisely, the density of deformation bands within the clusters appears to have increased as the clusters matured, suggesting progressive strain localization with increasing throw. Deformation band zones are expected to absorb most of the offset, and typically there is a limited number of deformation band zones within mature clusters compared with the number of single deformation bands.

Deformation band frequency v. layer thickness

Whereas spacing of joints typically is inversely proportional to the thickness of the fractured layer (e.g., Huang & Angelier 1989; Narr & Suppe 1991), Heynekamp *et al.* (1999) found that thick sandstones have wider damage zones with more deformation bands than thin sandstones. Motivated

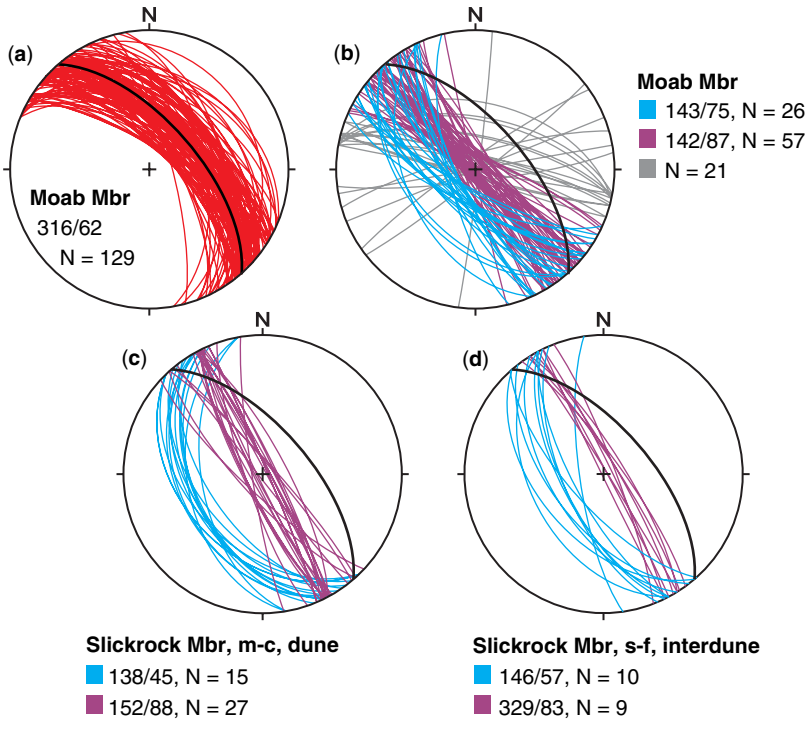

Fig. 11. Stereoplots (equal area, lower hemisphere) of deformation band orientations in the damage zone of the Bartlett Fault in Hidden Canyon, based on scanline data from the (**a** and **b**) Moab Member, (**c**) Slickrock Member dune, and (**d**) Slickrock Member interdune. The main fault (thick black line) is oriented at 318/62.

by this finding we compared the maximum deformation band frequency of deformation band clusters in the eolian sandstones with thickness in the range of about 1–25 m, based on data from 12 different scanlines. The results (Fig. 17a) demonstrate distinctly lower maximum deformation band frequency of clusters in the thinnest (1.3–1.8 m) layers compared with that of clusters in layers thicker than 3 m. Further, the maximum deformation band frequency of clusters in layers thicker than 3 m appears to be more or less unrelated to layer thickness.

These observations indicate an overall positive nonlinear or bilinear correlation between layer

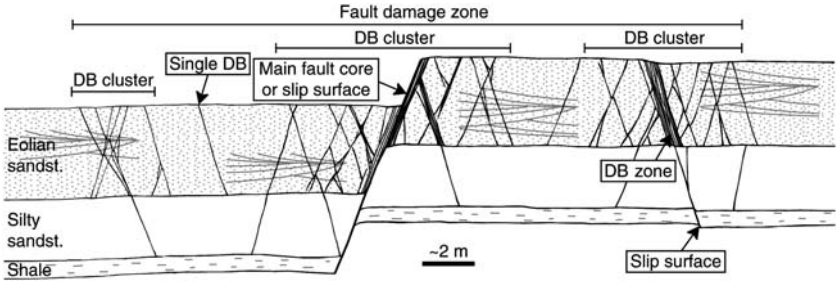

Fig. 12. Conceptual sketch of fault damage zones in the examined lithologies. Deformation bands dominate damage zones in eolian sandstones and appear as 1–2 mm wide isolated deformation bands or centimetres-wide tabular deformation band zones with densely packed deformation bands. Deformation bands and deformation band zones may also be concentrated at a larger (1–10 m) scale, here referred to as deformation band clusters. Fault damage zones may consist of several deformation band clusters. Deformation band clusters are nearly absent in the siltstones and shales.

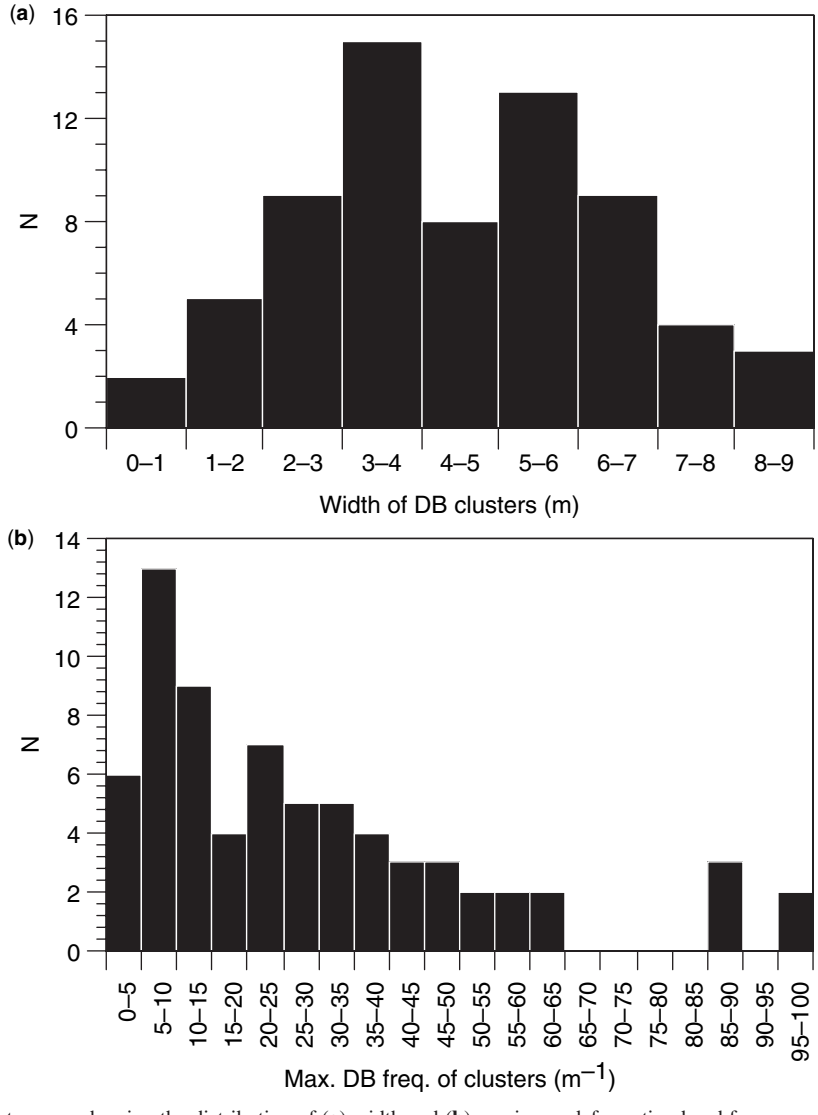

Fig. 13. Histograms showing the distribution of (**a**) width and (**b**) maximum deformation band frequency of deformation band clusters in the eolian sandstones. The maximum deformation band frequency denotes the highest concentration of bands (m^{-1}) within the deformation band clusters as recorded along the scanline.

thickness and maximum deformation band frequency, which can be attributed to the process of faulting in these and similar eolian sandstones. Growth of deformation band clusters in the eolian sandstones results mainly from strain hardening of gouge prior to faulting, but is expected to cease when slip surfaces nucleate. Deformation band zones represent the main contribution to high deformation band frequencies within deformation band clusters. Cluster growth in the eolian sandstones inevitably requires that the layers remain structurally coherent across the future fault plane (slip surface) so that strain hardening and thus cluster growth may continue. Where offset exceeds layer thickness so that the sandstone layer is cut off and juxtaposed against a weaker lithology, such as a siltstone or shale, clusters may cease to develop before slip surface nucleation takes place within the sandstone. Field observations show that the largest deformation band zones typically have

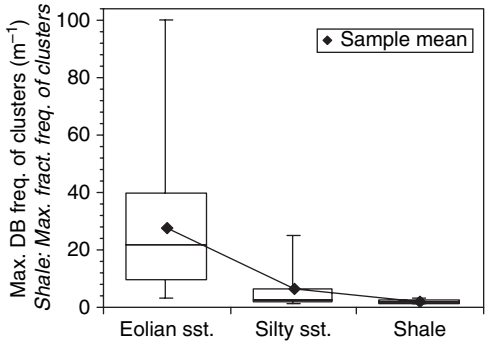

Fig. 14. Box plot with sample means showing the distribution of maximum deformation band (shale: fracture) frequency (m^{-1}) of deformation band clusters in eolian sandstones and siltstones, in addition to maximum fracture frequencies of fracture clusters in shales. The bottom and top of the boxes show the 25 and 75 percentiles, respectively, whereas the central horizontal lines show the median. Horizontal lines joined to the boxes by solid vertical lines represent the maximum and minimum values of the data set.

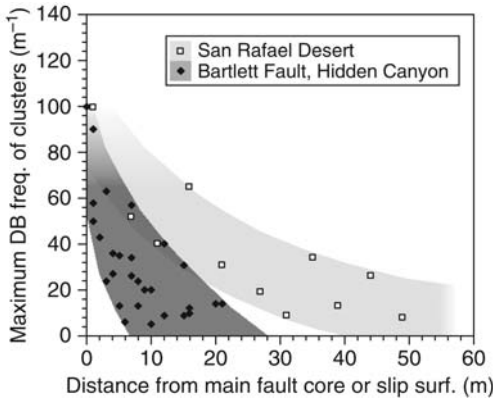

Fig. 15. Maximum deformation band (DB) frequency (m^{-1}) of deformation band clusters as a function of the distance from the main fault core or slip surface. The wide damage zone of the *c*. 200 m throw Bartlett Fault is compared with the narrower damage zones of the relatively small (<15 m throw) faults in the San Rafael Desert. Proximal to the main fault the deformation band frequency reaches a maximum of about 100 m^{-1}, suggesting a critical strain level where clusters become saturated with deformation bands and which seems independent of main fault offset. Together with cluster maturation close to the main fault, new clusters may form peripherally and increase the width of the damage zone.

accumulated decimetre-scale offset, and those associated with throughgoing slip surfaces have a total offset of the order of 0.5 m. Accordingly, growth of deformation band zones and clusters should not be affected by layer thickness in sandstone layers thicker than about 0.5 m. However, Figure 17a shows that the maximum deformation band frequency is low also for the 1.3–1.8 m thick sandstone layers, suggesting that the sandstone layers need not necessarily be cut off in order for cluster growth to cease.

Strain hardening and deformation band formation only continue as long as there is sand–sand contact across a deformation band zone. Where sand is juxtaposed against shale, i.e., in the upper and lower parts of the sand layer, strain is expected to localize in the shale or along the shale-sandstone interface in the form of an overlying and an underlying slip surface. Because of the short distance between these slip surfaces, they are likely to connect through the thin sandstone before the deformation band zones becomes very thick. As such, stress concentration within the thin (1.3–1.8 m) sandstone layers induced by the interacting slip surface tips may have facilitated localization of deformation through more intensive grain size reduction and early slip surface formation compared with thick (<3 m) layers. Deformation band frequency profiles in Figure 9 support this assumption. Here, clusters in the thin sandstone layers have lower maximum deformation band frequencies than those in the thickest layer (Layer 11). Nonetheless, clusters in both thin and thick sandstone layers are associated with slip surfaces. The significance and implications of these differences with respect to microstructure and micromechanical behaviour have not been explored in the current study.

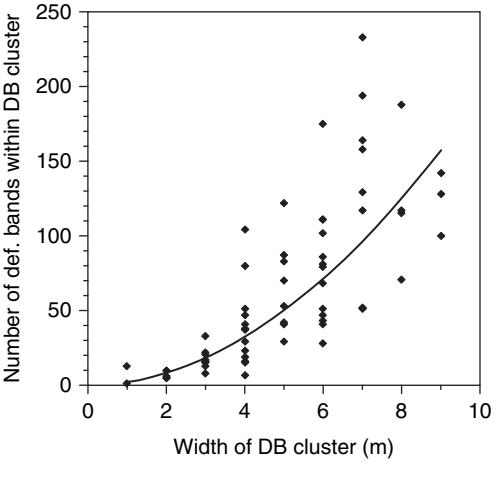

Fig. 16. Correlation of the total number of deformation bands (DBs) within the clusters against their respective widths indicates progressive localization of deformation with increasing offset.

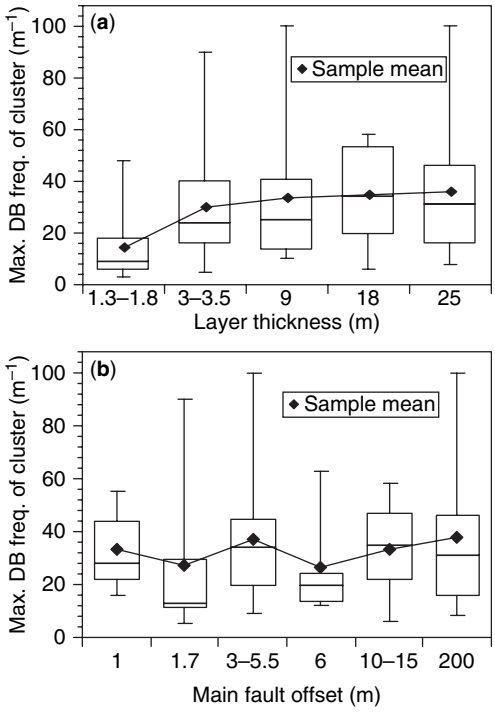

Fig. 17. Box plot of the maximum deformation band (DB) frequency of deformation band clusters in eolian sandstones correlated against (**a**) layer thickness and (**b**) main fault offset. Note that only sandstone layers thicker than 3 m were included in (**b**) to avoid influence of layer thickness on DB frequency. Eolian sandstone layers thinner than 2–3 m have less concentration of deformation bands compared with thicker layers. However, there is no strong correlation between deformation band frequency and layer thickness for layers thicker than 2–3 m in this lithology. Further, there is no apparent correlation between the maximum deformation band frequency of the deformation band clusters and main fault offset. See main text for discussion.

Deformation band frequency v. offset of main fault

The box plot in Figure 17b reveals no apparent correlation between the maximum deformation band frequency of the deformation band clusters in the eolian sandstones and main fault (slip surface or fault core) offset. Faults with offsets of about 1–200 m were incorporated. In order to isolate the effect of fault offset on the maximum deformation band frequency of the deformation band clusters, and because the deformation band frequency in thinner (<3 m) layers is affected by layer thickness (Fig. 17a), only data from layers with ≥ 3 m thickness were considered. The distribution of maximum deformation band frequencies associated with deformation band clusters is consistently skewed toward the lower values, regardless of main fault offset. In keeping with Figure 15, this finding indicates that formation of new clusters and maturation of existing clusters within the developing damage zone is more or less coeval. Thus, the lack of correlation between the maximum deformation band frequency and main fault offset points to a scale-invariant damage zone growth, where the accumulation of new deformation bands is approximately balanced by widening of the damage zone so that the distribution of the maximum deformation band frequency of the deformation band clusters remains more or less constant.

Deformation band and fracture orientation

In agreement with observations made by Aydin (1978) and Johnson (1995), the vast majority of the fault-related structures are oriented sub-parallel to their associated main fault (Figs 8–10). The fault-parallel deformation bands typically form two sets with opposing dip directions. These sets are either symmetric or slightly asymmetric about the vertical and mutually intersecting, suggesting that they originated as conjugate pairs. The dip is in the range of 50–80°. Sub-vertical deformation bands and shear fractures aligned with the main fault trend are also common. Conjugate, fault-parallel sets prevail in damage zones of isolated faults (e.g., Locality 1, San Rafael Desert) or isolated sections of faults where no significant mechanical fault interaction is evident.

There is a tendency for deformation bands to become more complexly oriented within sections of the damage zone that has the highest deformation band frequencies. Sets of deformation bands in the damage zone of the Bartlett Fault in Hidden Canyon show a wider range of orientations compared with deformation band sets in most of the damage zones of the small faults in the San Rafael Desert. Furthermore, sets of damage zone structures in the siltstones and shales are generally more distinct than sets in the eolian sandstones. Dense spacing of deformation bands, such as in mature deformation band clusters, may result in stress perturbations and mechanical interaction between deformation bands within the clusters, which in turn influence the orientation and geometry of the deformation bands (e.g., Fossen & Hesthammer 1997).

Mechanical interaction associated with fault branch points, fault overlap zones, and fault intersections may also result in stress perturbations and increased structural complexity (e.g., Cruikshank *et al.* 1991; Childs *et al.* 1995; Davatzes *et al.*

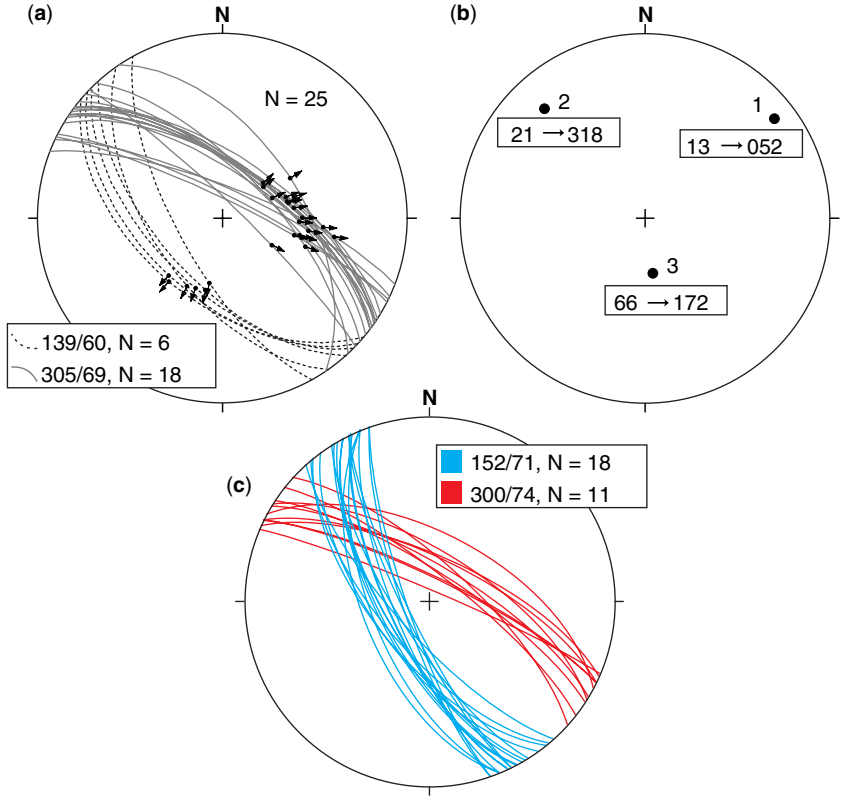

Fig. 18. (**a**) Orientation and slip lineation data of slip surfaces that breach the overlap zone in Locality 6, San Rafael Desert. (**b**) Palaeostress analysis indicates the maximum principal stress inclined at 25° from the vertical to the south (172°), whereas the least principal stress is oriented at 13/032 (Fig. 18). (**c**) Detailed mapping of deformation bands in unit e_1 along one of the breaching faults (Fig. 6) revealed similar orientations as the breaching faults, indicating that slip surfaces and associated deformation bands experienced a uniform stress field.

2005; Johansen *et al.* 2005) in order to accommodate differences in orientation and kinematics of the interacting faults. Locality 6 (Fig. 6) in the San Rafael Desert study area features an overlap zone, which is breached by numerous slip surfaces and associated deformation bands (Fossen *et al.* 2005). The breaching faults define two conjugate sets oriented at 139/60 and 305/69, obliquely to the overlapping faults (Fig. 18a). Palaeostress analysis of slip surface striations (P and T dihedral method, Angelier & Mechler 1977) internally in the overlap zone suggest that the maximum principal stress was inclined by 25° from the vertical to the south (172°), whereas the least principal stress was oriented at 13/032 (Fig. 18b). Detailed mapping of deformation bands in unit e_1 along one of the breaching faults (Fig. 6) revealed two sets of bands oriented sub-parallel to the oblique faults (Fig. 18c). This indicates that a uniform stress field prevailed during the formation of both the slip surfaces and associated deformation bands.

Accordingly, both stress perturbations resulting from mechanical interaction of faults as well as increasing structure density, such as in mature deformation band clusters proximal to the main fault or slip surface, seem to promote orientation heterogeneity within the damage zones examined.

Implications for fluid flow

Most deformation bands, and particularly those involving cataclasis, represent zones of reduced porosity and permeability (Pitman 1981; Antonellini & Aydin 1994; Gibson 1998; Heynekamp *et al.* 1999; Antonellini *et al.* 1999; Taylor & Pollard 2000; Lothe *et al.* 2002; Shipton *et al.* 2005; Sample *et al.* 2006). While deformation bands may locally reduce permeability by as

much as 5–6 orders of magnitude (e.g., Fisher & Knipe 2001), their effect on fluid flow in a petroleum reservoir is strongly dependent on their vertical and horizontal continuity and on their geometrical arrangement. Because transmissibility across the fault damage zone is a function of thickness and permeability only (e.g., Manzocchi *et al.* 1998), the number of deformation bands is an important parameter when considering cross-fault flow. However, where a producer or an injector is placed within the damage zone, the geometry and arrangement of the deformation bands become important. The conjugate sets mapped in the present study would favour fault-parallel flow controlled by deformation band clusters. Because the clusters are more well-developed close to the fault (Fig. 15), the location of the well with respect to the fault is important. Minor slip surfaces with low permeability perpendicular to strike (Antonellini & Aydin 1994) near the main fault, as observed in the damage zone of the Bartlett Fault (Fig. 10a), add to the low-permeable structure of the inner damage zone. However, slip surfaces often have significantly higher along-strike permeability, and may enhance transmissibility if the slip surfaces are interconnected and accessible to fluids.

The fact that the deformation bands are more frequent in the sandstones than in the more silty (still porous) layers may in some cases have a positive effect on reservoir performance. If present, deformation bands are likely to reduce the sweep in the most permeable sandstone layers and thereby counteract the expected early water-breakthrough in such intervals. One would expect this effect to increase with increasing amount of strain in the reservoir.

Conclusion

Detailed analyses of fault zones in interbedded porous sandstones, siltstones and shales have been conducted in order to examine internal fault zone geometry with emphasis on orientation and spatial distribution of fault-related deformation bands. Data from 29 scanlines were analyzed. The following conclusions were reached.

Deformation bands in fault damage zones in the sandstones are heterogeneously distributed in the form of individual bands, densely packed zones and clusters consisting of several zones. Conjugate sets of both bands and zones are common, but additional sets and increasing orientation heterogeneity occur close to the fault core and in complexly faulted areas. The maximum deformation band frequency of the deformation band clusters appears to decrease non-linearly away from the fault core so that clusters located near the fault must be expected to contain the highest concentrations of deformation bands. The data are consistent with the model that the maximum deformation band frequency in the damage zone is mainly established at the onset of faulting and that the syn-faulting increase in number of deformation bands is balanced by the widening of the damage zone.

Deformation bands zones and clusters are both thicker and more common in sandstones than in siltstones and are replaced by rare slip surfaces in shale layers. This difference is probably related to strain hardening: cataclastic deformation in the sandstone deformation bands involves significant strain hardening while granular flow in the siltstone deformation bands does not. However, thin (metres-thick) sandstone layers contain fewer deformation bands than thicker ones. This relation breaks down for a layer thickness of around 3 m in the study areas.

The authors are grateful to C. Childs and N. Davatzes for constructive and helpful reviews on an earlier version of this paper. Thanks also to Richard Kluge for assistance and company in the field. Richard Allmendinger's FaultKin program was used for the palaeostress analysis. The authors are thankful to StatoilHydro for funding the publication of this research.

References

ANGELIER, J. & MECHLER, P. 1977. Sur une methode graphique de recherche des contraintes principales egalement utilisable en tectonique et en seismologie: la methode des diedres droits. *Bulletin dela Societe Geologique de France*, **7**, 1309–1318.

ANTONELLINI, M. A. & AYDIN, A. 1994. Effect of faulting on fluid flow in porous sandstones: petrophysical properties. *American Association of Petroleum Geologists Bulletin*, **78**, 355–377.

ANTONELLINI, M. A. & AYDIN, A. 1995. Effect of faulting on fluid flow in porous sandstones: geometry and spatial distribution. *American Association of Petroleum Geologists Bulletin*, **79**, 642–671.

ANTONELLINI, M. A., AYDIN, A. & POLLARD, D. D. 1994. Microstructure of deformation bands in porous sandstones at Arches National Park, Utah. *Journal of Structural Geology*, **16**, 941–959.

ANTONELLINI, M. A., AYDIN, A. & ORR, L. 1999. Outcrop aided characterization of a faulted hydrocarbon reservoir: Arroyo Grande oil field, California, USA. *In*: HANEBERG, W. C., MOZLEY, P. S., MOORE, C. J. & GOODWIN, L. B. (eds) *Faults and Subsurface Fluid Flow*. American Geophysical Union Geophysical Monographs **113**, 7–26.

AYDIN, A. 1978. Small faults formed as deformation bands in sandstone. *In*: BYERLEE, J. D. & WYSS, M. (eds) *Rock Friction and Earthquake Prediction*. Birkhaeuser, Basel, 913–930.

AYDIN, A. & JOHNSON, A. M. 1978. Development of faults as zones of deformation bands and as slip surfaces in sandstone. *In*: BYERLEE, J. D. & WYSS, M. (eds) *Rock Friction and Earthquake Prediction*. Birkhaeuser, Basel, 931–942.

AYDIN, A. & JOHNSON, A. M. 1983. Analysis of faulting in porous sandstones. *Journal of Structural Geology*, **5**, 19–31.

AYDIN, A. & RECHES, Z. 1982. Number and orientation of fault sets in the field and in experiments. *Geology*, **10**, 107–112.

AYDIN, A., BORJA, R. I. & EICHHUBL, P. 2006. Geological and mathematical framework for failure modes in granular rock. *Journal of Structural Geology*, **28**, 83–98.

BEACH, A., WELBON, A. I., BROCKBANK, P. & MCCALLUM, J. E. 1999. Reservoir damage around faults: outcrop examples from the Suez rift. *Petroleum Geoscience*, **5**, 109–116.

BUMP, A. P. & DAVIS, G. H. 2003. Late Cretaceous–early Tertiary Laramide deformation of the northern Colorado Plateau, Utah and Colorado. *Journal of Structural Geology*, **25**, 421–440.

CAINE, J. S., EVANS, J. P. & FORSTER, C. B. 1996. Fault zone architecture and permeability structure. *Geology*, **24**, 1025–1028.

CASHMAN, S. & CASHMAN, K. 2000. Cataclasis and deformation-band formation in unconsolidated marine terrace sand, Humboldt County, California. *Geology*, **28**, 111–114.

CHILDS, C., WATTERSON, J. & WALSH, J. J. 1995. Fault overlap zones within developing normal fault systems. *Journal of the Geological Society of London*, **152**, 535–549.

CRUIKSHANK, K. M., ZHAO, G. & JOHNSON, A. M. 1991. Analysis of minor fractures associated with joints and faulted joints. *Journal of Structural Geology*, **13**, 865–886.

DAVATZES, N. C., EICHHUBL, P. & AYDIN, A. 2005. The structural evolution of fault zones in sandstone by multiple deformation mechanisms; Moab fault, SE Utah. *Geological Societey of America Bulletin*, **117**, 135–148.

DAVIS, G. H. 1999. *Structural Geology of the Colorado Plateau Regional of Southern Utah, with Special Emphasis on Deformation Bands*. Geological Society of America Special Papers, **342**.

DOELLING, H. H. 1988. Geology of Salt Valley Anticline and Arches National Park, Grand County, Utah. *In*: DOELLING, H. H., OVIATT, C. G. & HUNTOON, P. W. (eds) *Salt Deformation in the Paradox Region*. Utah Geological and Mineral Survey, Salt Lake City, UT, 1–58.

DOELLING, H. H. 2000. Geology of Arches National Park, Grand County, Utah. *In*: SPRINKEL, D. A., CHIDSEY, T. C. JR & ANDERSON, P. B. (eds) *Geology of Utah's Parks and Monuments*. Utah Geological Association, Salt Lake City, UT, 11–36.

DOELLING, H. H. 2001. *Geologic Map of the Moab and Eastern Part of the San Rafael Desert 30′ × 60′ Quadrangles, Grand and Emery Counties, Utah, and Mesa County, Colorado*. Geologic Map **180**. Utah Geological Survey, Salt Lake City, UT.

DOELLING, H. H. 2002. *Geologic Map of the Fisher Towers 7.5′ Quadrangle, Grand County, Utah*. Utah Geological Survey, Salt Lake City, UT, 22, 1 Sheet.

DU BERNARD, X., EICHHUBL, P. & AYDIN, A. 2002. Dilation bands: a new form of localized failure in granular media. *Geophysical Research Letters*, **29**, 2176–2179.

FISHER, Q. J. & KNIPE, R. J. 1998. Fault sealing processes in siliciclastic sediments. *In*: FISHER, Q. J. & KNIPE ROBERT, J. (eds) *Faulting, Fault Sealing and Fluid Flow in Hydrocarbon Reservoirs*. The Geological Society of London, Special Publications, **147**, 117–134.

FISHER, Q. J. & KNIPE, R. J. 2001. The permeability of faults within siliciclastic petroleum reservoirs of the North Sea and Norwegian Continental Shelf. *Marine and Petroleum Geology*, **18**, 1063–1081.

FISHER, Q. J., CASEY, M., HARRIS, S. D. & KNIPE, R. J. 2003. Fluid flow properties of faults in sandstone: the importance of temperature history. *Geology*, **31**, 965–968.

FOSSEN, H. & HESTHAMMER, J. 1997. Geometric analysis and scaling relations of deformation bands in porous sandstone from the San Rafael Desert, Utah. *Journal of Structural Geology*, **19**, 1479–1493.

FOSSEN, H., JOHANSEN, T. S. E., HESTHAMMER, J. & ROTEVATN, A. 2005. Fault interaction in porous sandstone and implications for reservoir management; examples from southern Utah. *American Association of Petroleum Geologists Bulletin*, **89**, 1593–1606.

FOSSEN, H., SCHULZ, R. A., SHIPTON, Z. K. & MAIR, K. 2007. Deformation bands in sandstone – a review. *Journal of the Geological Society of London*, **164**, 755–769.

FOWLES, J. & BURLEY, S. 1994. Textural and permeability characteristics of faulted, high porosity sandstones. *Marine and Petroleum Geology*, **11**, 608–623.

FOXFORD, K. A., GARDEN, I. R., GUSCOTT, S. C., BURLEY, S. D., LEWIS, J. L. L., WALSH, J. J. & WATTERSON, J. 1996. The Field Geology of the Moab Fault. *In*: HUFFMAN, A. C., LUND, W. R. J. & GODWIN, L. H. (eds) *Geology and Resources of the Paradox Basin*. Utah Geological Association, Salt Lake City, UT, 265–283.

GARDEN, I. R., GUSCOTT, S. C., BURLEY, S. D., FOXFORD, K. A., WALSH, J. J. & MARSHALL, J. 2001. An exhumed palaeo-hydrocarbon migration fairway in a faulted carrier system, Entrada Sandstone of SE Utah, USA. *Geofluids*, **1**, 195–213.

GIBSON, R. G. 1998. Physical character and fluid-flow properties of sandstone-derived fault zones. *In*: COWARD, M. P., JOHNSON, H. & DALTABAN, T. S. (eds) *Structural Geology in Reservoir Characterization*. Geological Society, London, Special Publications, **127**, 83–97.

HADIZADEH, J. & JOHNSON, W. K. 2003. Estimating local strain due to comminution in experimental cataclastic textures. *Journal of Structural Geology*, **25**, 1973–1979.

HARPER, T. R. & LUNDIN, E. R. 1997. Fault seal analysis: reducing our dependence on empiricism. *In*: MÖLLER-PEDERSEN, P. & KOESTLER, A. G. (eds)

Hydrocarbon Seals – Importance for Exploration and Production. 7. Norwegian Petroleum Society Special Publications, **7**, 149–165.

HESTHAMMER, J. & FOSSEN, H. 2000. Uncertainties associated with fault sealing analysis. *Petroleum Geoscience*, **6**, 37–45.

HESTHAMMER, J. & FOSSEN, H. 2001. Structural core analysis from the Gullfaks area, northern North Sea. *Marine and Petroleum Geology*, **18**, 411–439.

HESTHAMMER, J., BJØRKUM, P. A. & WATTS, L. 2002. The effect of temperature on sealing capacity of faults in sandstone reservoirs; examples from the Gullfaks and Gullfaks Sør fields, North Sea. *American Association of Petroleum Geologists Bulletin*, **86**, 1733–1751.

HEYNEKAMP, M. R., GOODWIN, L. B., MOZLEY, P. S. & HANEBERG, W. C. 1999. Controls on fault-zone architecture in poorly lithified sediments, Rio Grande Rift, New Mexico; implications for fault-zone permeability and fluid flow. *In*: HANEBERG, W. C., MOZLEY, P. S., MOORE, J. C. & GOODWIN, L. B. (eds) *Faults and Subsurface Fluid Flow in the Shallow Crust*. American Geophysical Union, Washington, DC, 27–49.

HUANG, Q. & ANGELIER, J. 1989. Fracture spacing and its relation to bed thickness. *Geological Magazine*, **126**, 355–362.

JAMISON, W. R. & STEARNS, D. W. 1982. Tectonic deformation of Wingate Sandstone, Colorado National Monument. *American Association of Petroleum Geologists Bulletin*, **66**, 2584–2608.

JOHNSON, A. M. 1995. Orientations of faults determined by premonitory shear zones. *Tectonophysics*, **247**, 161–238.

JOHANSEN, T. E. S., FOSSEN, H. & KLUGE, R. 2005. The impact of syn-faulting porosity reduction on damage zone architecture in porous sandstone; an outcrop example from the Moab Fault, Utah. *Journal of Structural Geology*, **27**, 1469–1485.

KNIPE, R. J., FISHER, Q. J. *ET AL*. 1997. Fault seal analysis: successful methodologies, application and future directions. *In*: MØLLER-PEDERSEN, P. & KOESTLER, A. G. (eds) *Hydrocarbon Seals: Importance for Exploration and Production*. Norwegian Petroleum Society Special Publications, **7**. Elsevier, Singapore, 15–40.

LOTHE, A. E., GABRIELSEN, R. H., BJØRNEVOLL-HAGEN, N. & LARSEN, B. T. 2002. An experimental study of the texture of deformation bands; effects on the porosity and permeability of sandstones. *Petroleum Geoscience*, **8**, 195–207.

MAIR, K., MAIN, I. & ELPHICK, S. 2000. Sequential growth of deformation bands in the laboratory. *Journal of Structural Geology*, **22**, 25–42.

MANDL, G., DE JONG, L. N. J. & MALTHA, A. 1977. Shear zones in granular material. *Rock Mechanics*, **9**, 95–144.

MANZOCCHI, T., RINGROSE, P. S. & UNDERHILL, J. R. 1998. Flow through fault systems in high-porosity sandstones. *In*: COWARD, M. P., JOHNSON, H. & DALTABAN, T. S. (eds) *Structural Geology in Reservoir Characterization*. The Geological Society of London, Special Publications, **127**, 65–82.

MARONE, C. & SCHOLZ, C. H. 1989. Particle-size distribution and microstructures within simulated fault gouge. *In*: SPRAY, J. G. & HUDLESTON, P. J. (eds) *Friction Phenomena in Rock*. Pergamon, Oxford, 799–814.

MENÉNDEZ, B., ZHU, W. & WONG, T. F. 1996. Micromechanics of brittle faulting and cataclastic flow in Berea Sandstone. *Journal of Structural Geology*, **18**, 1–16.

MILLIGAN, M. R. 2000. Geology of Goblin Valley State Park, Utah. *In*: SPRINKEL, D. A., CHIDSEY, T. C., JR. & ANDERSON, P. B. (eds) *Geology of Utah's Parks and Monuments*. Utah Geological Association, Salt Lake City, UT, 11–36.

NARR, W. & SUPPE, J. 1991. Joint spacing in sedimentary rocks. *Journal of Structural Geology*, **13**, 1037–1048.

NUCCIO, V. F. & CONDON, S. M. 1996. *Burial and Thermal History of the Paradox Basin, Utah and Colorado, and Petroleum Potential of the Middle Pennsylvanian Paradox Basin*. US Geological Survey, Reston, VA.

OWEN, G. 1987. Deformation processes in unconsolidated sands. *In*: JONES, M. E. & PRESTON, R. M. (eds) *Deformation of Sediments and Sedimentary Rocks*. The Geological Society of London, Special Publications, **29**, 11–24.

PEVEAR, D. R., VROLIJK, P. J. & LONGSTAFFE, F. J. 1997. Timing of Moab fault displacement and fluid movement integrated with burial history using radiogenic and stable isotopes. *In*: HENDRY, J. P., CAREY, P. F. & PARNELL, J. (eds) *Geofluids II '97, Contributions to the Second International Conference on Fluid Evolution, Migration and Interaction in Sedimentary Basins and Orogenic Belts*. 10–14 March 1997, Belfast: Queen's University of Belfast, 42–45.

PITTMAN, E. D. 1981. Effect of fault-related granulation on porosity and permeability of quartz sandstones, Simpson Group (Ordovician) Oklahoma. *American Association of Petroleum Geologists Bulletin*, **65**, 2381–2387.

RAWLING, G. C. & GOODWIN, L. B. 2003. Cataclasis and particulate flow in faulted, poorly lithified sediments. *Journal of Structural Geology*, **25**, 317–331.

SAMPLE, J. C., WOODS, S., BENDER, E. & LOVEALL, M. 2006. Relationship between deformation bands and petroleum migration in an exhumed reservoir rock, Los Angeles Basin, California, USA. *Geofluids*, **6**, 105–112.

SCHULTZ, R. A. & FOSSEN, H. 2002. Displacement-length scaling in three dimensions; the importance of aspect ratio and application to deformation bands. *Journal of Structural Geology*, **24**, 1389–1411.

SCHULTZ, R. A. & SIDDHARTHAN, R. 2005. A general framework for the occurrence and faulting of deformation bands in porous granular rocks. *Tectonophysics*, **411**, 1–18.

SHIPTON, Z. K. & COWIE, P. A. 2001. Damage zone and slip-surface evolution over μm to km scales in high-porosity Navajo sandstone, Utah. *Journal of Structural Geology*, **23**, 1825–1844.

SHIPTON, Z. K. & COWIE, P. A. 2003. A conceptual model for the origin of fault damage zone structures in high-porosity sandstone. *Journal of Structural Geology*, **25**, 333–344.

SHIPTON, Z. K., EVANS, J. P. & THOMPSON, L. B. 2005. The geometry and thickness of deformation-band fault core and its influence on sealing characteristics of

deformation-band fault zones. *American Association of Petroleum Geologists Memoir*, **85**, 181–195.

SOLUM, J. G., VAN DER PLUIJM, B. A. & PEACOR, D. R. 2005. Neocrystallization, fabrics and age of clay minerals from an exposure of the Moab Fault, Utah. *Journal of Structural Geology*, **27**, 1563–1576.

TAYLOR, W. L. & POLLARD, D. D. 2000. Estimation of in situ permeability of deformation bands in porous sandstone, Valley of Fire, Nevada. *Water Resources Research*, **36**, 2595–2606.

UNDERHILL, J. R. & WOODCOCK, N. H. 1987. Faulting mechanisms in high-porosity sandstones; New Red Sandstone, Arran, Scotland. *In*: JONES, M. E. & PRESTON, M. F. (eds) *Deformation of Sediments and Sedimentary Rocks*. The Geological Society, London, 91–105.

WIBBERLEY, C. A. J., PETIT, J. P. & RIVES, T. 2000. Mechanics of cataclastic 'deformation band' faulting in high-porosity sandstone, Provence. *Comptes Rendus de l'Academie des Sciences, Serie II. Sciences de la Terre et des Planetes*, **331**, 419–425.